Protein Desolvation in UV Matrix-Assisted Laser Desorption/Ionization (MALDI)

Emmanuelle Sachon,[a,b] Gilles Clodic,[b] Thierry Blasco,[b] and Gérard Bolbach[a,b]

[a] Université Pierre et Marie Curie, UMR 7613 CNRS, Structure et Fonction de Molécules Bioactives, Paris, France
[b] UPMC, Plate-Forme Spectrométrie de Masse et Protéomique, (IFR83), Paris, France

We describe experiments in MALDI-TOF and MALDI-TOF-TOF showing that the ejection of protein-matrix cluster ions and their partial decay in the source occur in MALDI. The use of radial beam deflection and small size detector in linear mode allows detection of ions with higher time-of-flight and kinetic energy deficit. MALDI-TOF-TOF experiments were carried out by selecting chemical noise ions at *m/z* higher than that of a free peptide ion. Whatever the selected *m/z* (up to *m/z* 300) the molecular peptide ion appeared as the main fragment. The production of protein-matrix clusters and their partial decay in the source was found to increase with the size of the protein (MW from 1000 to 150,000 u), although it decreases with increasing charge state. These effects were observed for different matrices (HCCA and SA) and in a large laser fluence range. Experimental results and calculation highlight that a continuous decay of protein-matrix cluster ions occurs in the source. This decay-desolvation process can account for the high-mass tailing and peak shifting as well as the strong noise/background in the mass spectra of proteins. (J Am Soc Mass Spectrom 2007, 18, 1880–1890) © 2007 American Society for Mass Spectrometry

Matrix-assisted laser desorption/ionization (MALDI) was introduced in the mid 1980s by Karas and Hillenkamp [1]. This new ionization method allows the production of large intact molecular ions (protein, peptide, DNA, synthetic polymer, etc.) in the gas phase. Intact ions are then analyzed by a mass analyzer, essentially time-of-flights (TOFs).

Although MALDI-TOF is now a well-established and powerful method, many questions are still open concerning (1) the conditions of a successful experiment and (2) the main mechanisms involved in the formation of free intact ions [2].

Target preparation is a critical step in MALDI. Analyte is often supposed to be co-crystallized with a large excess of matrix. This incorporation of analyte into the small matrix crystals (co-crystallization) remains an open question [3, 4]. However, a protein in the target is likely surrounded by matrix molecules.

The ejection of material in the very first stage leads to a very dense plume (with a density similar to that of the target) becoming increasingly more diluted (gas) during the plume expansion.

The main question is how a free ion is formed from such a dense plume and why analyte-matrix clusters are not the main products. Ejection of matrix-analyte clusters was already found as essential for the analyte ionization in MALDI [5–8]. Desorption of large clusters was also predicted from molecular dynamics simulations [9, 10]. Other authors believe that ionization can be explained by an ion-molecule reaction in the plume [11]. Recent very interesting simulations, including desorption/ablation molecular dynamics and ionization processes modeling, showed that free ions and those in clusters are produced with close abundance in the plume [12].

The ion analysis through axial-TOF instruments is probably the key point of the main observation of free ions in MALDI. A free ion formed in the source before the delay time is fully accelerated and is detected at a given time forming a resolved peak. The peak width is a function of the initial axial velocity depending on the matrix and the delayed extraction conditions. The time-of-flight is quantitatively associated with the ion *m/z*. In linear mode, a decay of the free ion in the drift tube through metastable decomposition changes only the peak width but not the centroid.

For ions resulting from an early decay of clusters in the source, the time-of-flight is not directly correlated to the initial *m/z* of the cluster ion. Depending on the clusters size and the decay parameters, the time-of-flight of detected ions can be observed in a large range as unresolved peaks. This includes matrix clusters and analyte-matrix clusters. Using an ion trap, Krutchinsky and Chait showed that matrix cluster ions were detected by MS/MS at practically every *m/z* [13]. These matrix cluster ions are responsible for the so-called chemical noise background. In these MALDI-ion trap

Address reprint requests to Dr. Gérard Bolbach, UPMC, Plate-Forme Spectrométrie de Masse et Protéomique, (IFR83), case courrier 41, 7-9 Quai Saint-Bernard 75252 Paris Cedex 05, France. E-mail: bolbach@ccr.jussieu.fr

1044-0305/07/$32.00
doi:10.1016/j.jasms.2007.07.029

Published online August 3, 2007
Received March 13, 2007
Revised May 29, 2007
Accepted July 30, 2007

experiments, acceleration, ion transfer, and trapping times are much higher (~1 s) than the ion time-of-flight in MALDI-TOF (~100 μs). Thus, matrix cluster ions will also be a major component of the chemical noise in MALDI-TOF. The overall noise in MALDI, through unresolved ions, was estimated to the largest fraction of the charges produced in MALDI [14].

Protein mass spectra acquired in MALDI-TOF exhibit not only a high level of chemical noise but also more or less symmetric protein peaks with extended tails. Cation adducts and photochemical adducts of matrix or matrix fragments to the analyte ion were reported in the early days of MALDI-TOF and can contribute to this tailing [15]. Any decay of the free analyte ion in the source would produce signals at lower time-of-flights and thus cannot account for this tailing.

The extended tail of the protein ion peak is a major drawback in determining its precise molecular weight. In this study we reinvestigate the origin of this tailing effect through the possible decay-desolvation of analyte-matrix cluster ions in the MALDI source.

Decay-desolvation of analyte-matrix cluster ions in the source can in principle produce ions (free protein ions and lower mass cluster ions) with time-of-flight starting with that of the free ion and with an extension to higher time-of-flights (referred to here as a high-mass tailing). Free protein ions are characterized by a full kinetic energy (complete acceleration), whereas in-source decay analyte-matrix cluster ions are characterized by a kinetic energy deficit.

MALDI-TOF experiments in linear mode using an off-line detector and radial deflection plates before detection were carried out to study the effect of the kinetic energy deficit. The origin of the chemical noise beyond the peptide free ion peaks was studied by tandem mass spectrometry (MALDI-TOF-TOF) experiments. Our results show that ions produced by the decay of analyte-matrix clusters in the source can account for the protein high-mass tailing and chemical noise. Some models of decay-desolvation are discussed.

Experimental

Materials

Matrices, α-cyano-4-hydroxycinnamic acid (HCCA) and sinapinic acid (SA), (from Applied Biosystems) were used as saturated solutions in acetonitrile/water/TFA 1/1/0.1%. Standard proteins [bovine serum albumin (BSA), immuniglobulin IgG1, a mixture of horse skeletal apomyoglobin, thioredoxin, and bovine insulin] and peptides [des-Arg [1]-Bradykinin, angiotensinI, Glu1-Fibrinopeptide B, ACTH 1–17, ACTH 18–39, ACTH 7–38 (from Applied Biosystems)] mixture solutions were dissolved in water/0.1% TFA.

Samples were prepared by standard dried-droplet method. Typically 0.02 to 3 pmol of peptides and 2 to 4 pmol of proteins were deposited on a 192 positions plate.

Instrumentation

MALDI-TOF linear mode. MALDI-TOF experiments were performed on a MALDI-TOF-TOF (4700 Proteomics Analyzer, Applied Biosystems) using the linear mode and delayed extraction. A diode-pumped Nd:YAG laser (λ = 355 nm, 15 μJ) operated at 200 Hz. This mass spectrometer was described previously [16, 17]. It should be mentioned that this mass spectrometer was designed for MS/MS studies of peptides and the linear mode was optional. The ion optics after the ion source (dual stages without grids) are composed of three different deflection plates (X1Y1, X2Y2, X3Y3) and two Einzel lenses (Ez1, Ez2) to focus the ion beam along the axis of the TOF analyzer (z direction) (Figure 1A). The target voltage was set to 20 kV, the first electrode (El_1) was set at 18.6 kV, whereas the second (El_2) was grounded.

The apparent diameter of the laser spot was determined to be 75 μm at high energy. Experiments were carried out at a laser energy slightly higher than the threshold, thus allowing production of protein ions and signal detection.

In the linear mode, the ion detector, composed of two microchannel plates of low diameter (useful diameter ≃ 18 mm), is off-axis in the y direction (Figure 1B). The distance between the deflector Y3 and the plane of the detector is about 84 cm; the off-line distance is about 2 cm.

In these experiments, the MALDI-TOF mass spectra were recorded as a function of the voltages applied on the X3 deflector (−450 V, +450 V) with VY3 ≃ 165 V and on the Y3 deflector (0 V, +450 V) with VX3 = 0. The voltages VY3 ≃ 165 V and VX3 ≃ 0 V correspond to the optima for detection of free ions, as expected from the distances and applied voltages. In total, 19 or 21 steps were used to cover the range of VX3 or VY3.

Due to the variability of shot to shot and sample to sample in MALDI, these experiments were performed on a large number of samples (a few thousands). Each mass spectrum resulted from the average of mass spectra recorded on at least 50 random spots on the target with 50 to 150 laser shots per spot.

Ion deflection before detection is essentially characterized by the deflection angle α (Figure 1B) depending on the ion charge state z, the kinetic energy E_k, and the parameters of the deflector: V_d, the deflection voltage; L, the length of the electrodes; and D, the distance between the electrodes according to the following formula. In this formula the radial velocity component is neglected compared to the axial velocity.

$$\mathrm{Tan}\left(\alpha\right) \sim 0.5 z e V_d L/(E_k D) \quad (1)$$

From this formula, the angle of deflection α is identical for all the free ions leaving the target (E_k = zeVacc = ½ mv^2) or cluster ions undergoing a complete decay in the source, just before the delay time of extraction. Thus the deflection voltage (V_d) range is the same for the singly and multiply charged free ions. For ions resulting from

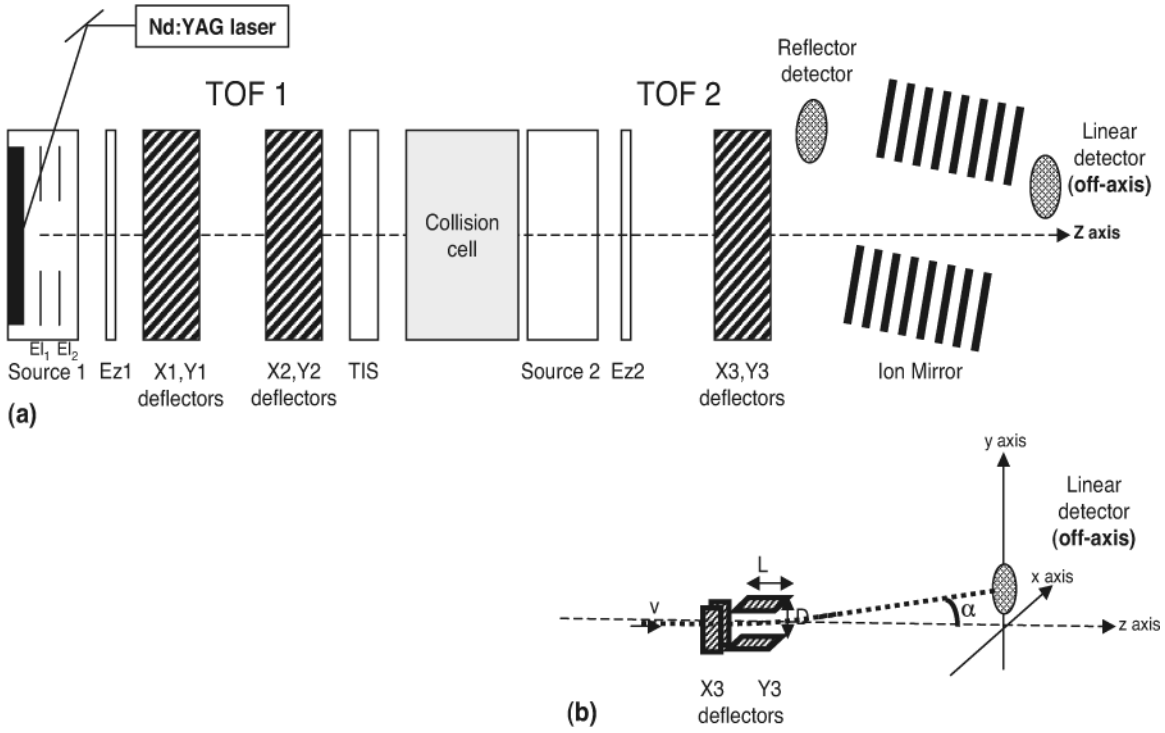

Figure 1. (**a**) Schematic view of the MALDI-TOF-TOF apparatus. El_1 and, El_2: extraction electrodes in the source, Ez1: Einzel lenses 1, Ez2: Einzel lenses 2, TIS: Time Ion Selector. (**b**) Schematic view of the deflection plates X3 (horizontal) and Y3 (vertical) and the off-axis detector.

a partial decay-desolvation of cluster ions in the source, the kinetic energy E'k is smaller than E_k and the deflection voltage range is different.

MALDI-TOF-TOF. This tandem time-of-flight was previously described in detail by Vestal et al. [17]. The ions produced in the source 1 were accelerated by 8 kV. Ions of interest were time selected in the Time Ion Selector (TIS) (Figure 1a). The chosen mass window was (−1 u, +10 u) for a given *m/z* value of the singly charged precursor ion. Then, ions were decelerated to enter the collision cell (empty or filled with N_2 gas at pressure 2×10^{-7} Torr) with a kinetic energy of 1 keV. Parent and fragment ions travel with very close velocities to a pulsed accelerator (accelerating voltage = 18 kV), acting as a second source (Figure 1a). After reflection in the two-stage mirror they are detected. Because mirror geometry was not designed to reflect and analyze high mass protein ions, this study was mainly applied to peptide ions (ACTH 7–38, ACTH 18–39).

Results

Deflection Effect in Linear Mode with the HCCA Matrix

Vertical deflection. The positive-ion mass spectra of peptides and proteins were recorded as a function of the radial deflection voltages VY3 (VX3 = 0 V) using HCCA as the matrix. Two main features can be noted on the typical mass spectra observed for BSA as a function of the deflector voltages VY3 (Figure 2a).

First, mass spectra acquired for VY3 in the range of 135–338 V showed the molecular peak of BSA^{+1} with a tailing shifted toward higher *m/z*. This VY3 range is in relatively good agreement with that calculated for full kinetic energy ions, i.e., VY3 ≃ 110–250 V, taking into account the geometry of the deflector-detector device and assuming an ion beam without radial dispersion (position and velocity). The tails, hereafter named Distribution I, are also noted in a lesser extent for the higher charge states of BSA^{+n} ions (Figure 2a–c). For VY3 values of 292 and 338 V the free ion peak and the Distribution I are clearly decoupled. At the extreme deflection voltages (VY3 values of < 90 and >338 V), no free ions were detected and one or two broad and shifted peaks (Distribution II) are present, especially for the lower charge states BSA^{+1} and BSA^{+2} (Figure 2a–c). Kinetic energy of the ions is lower for Distribution II than for Distribution I.

Second, the tailing effect is more important for BSA^{+1} than for the highest charge states ($n > 3$). Figure 3a and b show the variation of the centroid and abundance of the free ion BSA^{+1} and the Distributions I and II as a function of the VY3 voltages. These data were averaged over four different experiments. No peak deconvolution was applied for the Distribution I and the free ion. The centroid and peak area were estimated by integrating the signal in the *m/z* range of the resolved

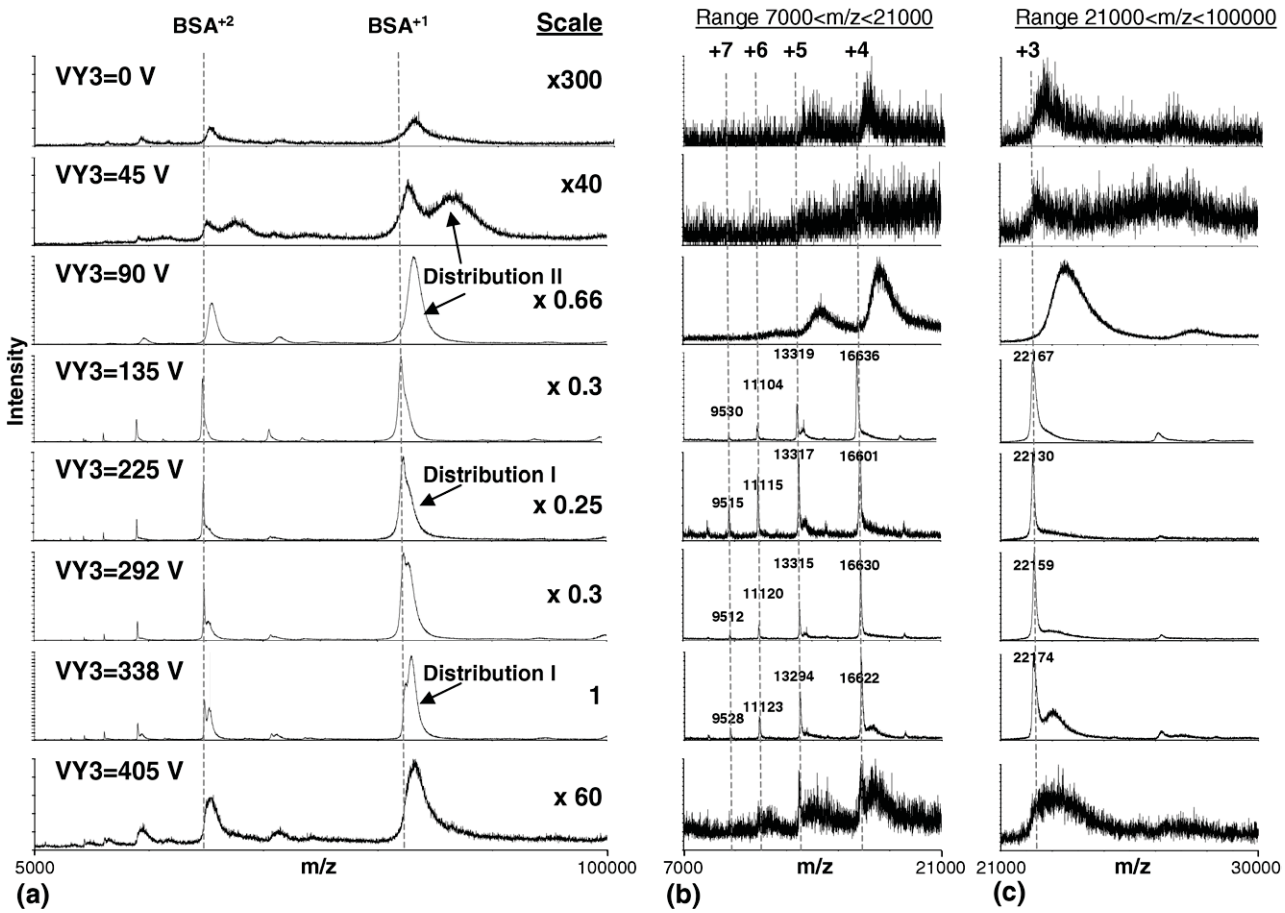

Figure 2. (**a**) Typical positive ion BSA MALDI mass spectra ($5000 < m/z < 100{,}000$) recorded as a function of the deflection voltage VY3 (VX3 = 0). Each mass spectrum is the average of 100–200 laser shots on 50 random spots on the target. The delay time was set to 1490 ns and HCCA was used as the matrix. The right scale indicates the maximum of ion signal relatively to the most intense (taken as the unit) obtained for VY3 = 338 V. (**b**) Expansion of partial mass spectra in the m/z range of BSA^{4+} to BSA^{+7} ($7000 < m/z < 21{,}000$) and (**c**) in the m/z range of BSA^{+3} ($21{,}000 < m/z < 30{,}000$). Dashed lines show the expected peak for singly and multiply charged BSA free ions.

peak and tailing, respectively. It should be mentioned that the overall signal of the free ion is lower than that of the tail for BSA^{+1}. However, it is higher for the higher charge states. These trends are even more pronounced for larger proteins such as IgG1 (data not shown).

Careful examination of the mass spectra also showed that one peak (hereafter named peak1) appeared at the end of tailing of the Distribution I (Figure 4). This peak was detected only when the free ion was observed with a similar width (Figure 3a). It should be noted that the m/z of peak1 does not correspond to any multiple charge of protein cluster ions.

All these features are quite reproducible and were noted for a few thousands of samples of each tested protein (IgG1, BSA, apomyoglobin, thioredoxin, and insulin). They were also found for peptides (Figure 5). Experiments on pure matrix without added analyte were also carried out and they gave similar trends. A broad distribution of very low abundance and shifted with respect to the $(m+H)^+$ and $(2m+H)^+$ free matrix ions was found for the extreme deflection voltages.

These observations were made over 18 months. Replacing the laser induced some minor changes in Distributions I and II with respect to the applied deflection voltages.

Horizontal deflection. The same effects and the same trends on the mass spectra of proteins were observed with the horizontal deflection voltage VX3. Free ions were detected in the VX3 range (−250 V, +250 V). This symmetric range is expected from the geometry and distances of the deflection-detection setup (−260 V, +260 V). Distributions I and II and peak1 were observed as depicted earlier for the vertical deflection. The abundance of Distributions I and II and free ion was also found to depend on the charge state (Figure 3c). The higher the charge state, the higher the free ion abundance. The abundance ratio [free ion/(free ion + distribution)] was about 0.5, 0.6, 0.7, 0.75, and 1 for

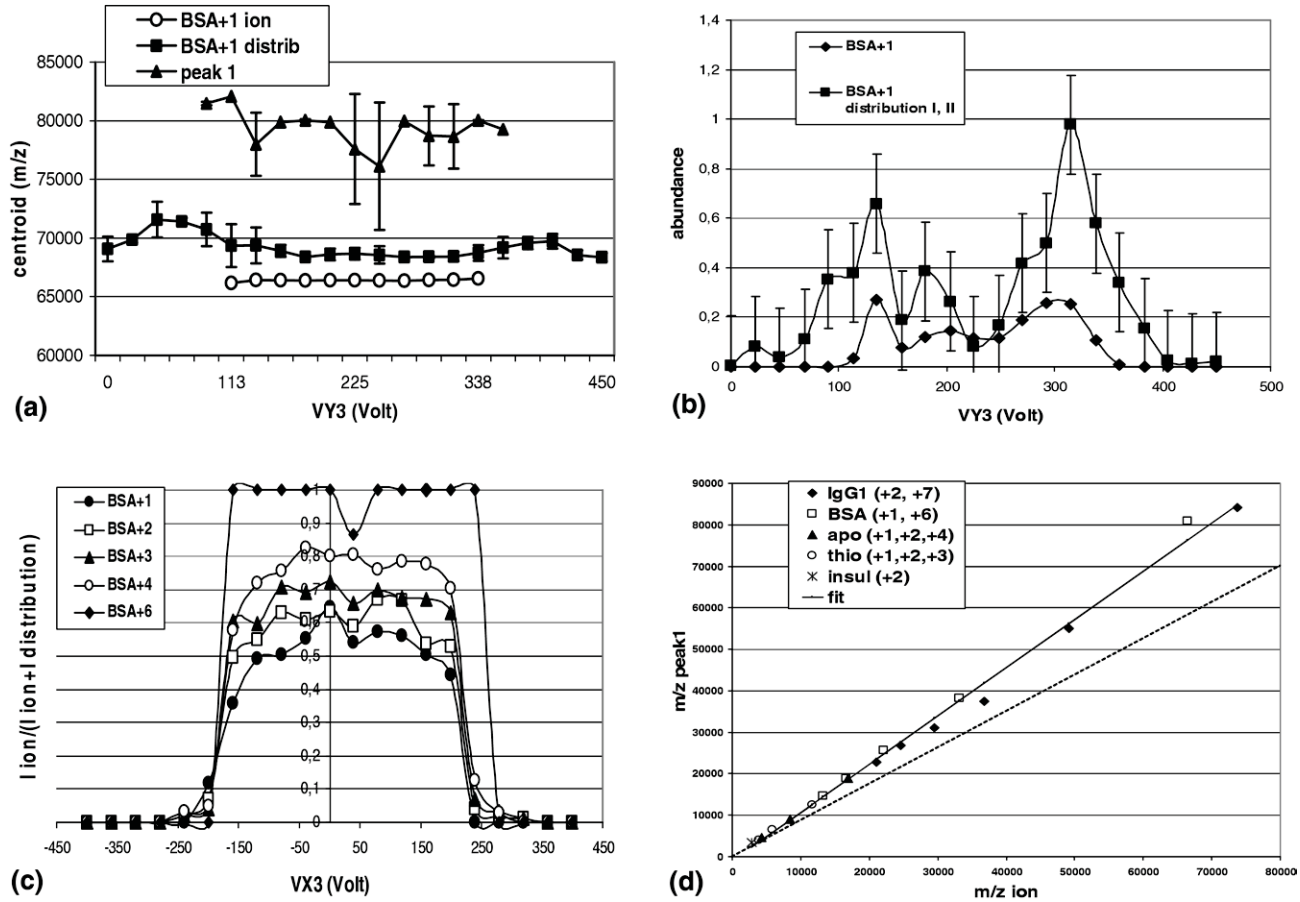

Figure 3. (**a**) Centroids of BSA^{+1} free ion (○), associated Distributions I and II (■), and peak1 (▲) as a function of the vertical deflection voltage VY3. (**b**) Abundance of BSA^{+1} free ion (◆) and associated Distributions I and II (■) as a function of the vertical deflection VY3. The abundances were normalized with respect to the highest peak area. (**c**) Abundance ratio $[I_{ion}/(I_{ion} + I_{distribution})]$ for BSA^{+n} [n = 1 (●), 2 (□), 3 (▲), 4 (○), and 6 (◆)], as a function of the horizontal deflection voltage VX3. (**d**) Plot of the peak1 as a function of the protein m/z [IgG1 (◆), BSA (□), Apomyoglobin (▲), Thioredoxin (○), Insulin (*)]. The full line indicates the linear fit on the experimental data (Equation: $m/z_{peak1} = 1.1637 \times (m/z_{ion}) - 954$). The dashed line corresponds to the slope 1.

BSA^{+1}, BSA^{+2}, BSA^{+3}, BSA^{+4}, and BSA^{+6}, respectively. For a given charge state, the free ion abundance is lower for larger proteins. The abundance ratio was about 0.5 and 0.8 for singly charged BSA and apomyoglobin, respectively.

Taking into account the data on peak1 for all the proteins and charge states, a linear relationship was found between the peak1 m/z and the free ion m/z (Figure 3d). Assuming that peak1 corresponds to a protein-matrix cluster free ion, these clusters would be composed of 60 and 20 HCCA molecules for m/z 77,000 and m/z 25,000, respectively. For $m/z < 5000$, the number of matrix molecules would be negligible.

Influence of the Delayed Extraction

The effects of the delay time (dt = 180, 820, and 1830 ns) on the typical mass spectra acquired for different deflection voltages (VX3 and VY3) were also studied. These delay times correspond to extraction of singly charged ions with the best resolution at m/z 2000, 20,000, and 100,000, respectively.

The delay time induces a minor decrease of ion kinetic energy. Compared to full accelerated ions (20 kV), the delay times dt = 180 ns and dt = 1830 ns would induce an energy deficit of 0.09 and 0.9%, respectively, with a mean initial axial velocity of 350 m/s (HCCA). However the delay time has an important role, considering that the ions could be accelerated in a dense or more diluted plume. For the shorter delay time (dt = 180 ns), ions should be accelerated in a very dense plume and more collisions with neutral matrix molecules are expected.

These results showed two different situations. No systematic effect of the delay time was noted for the free ions. The free ions and Distribution I were shifted toward higher time-of-flights with increasing delay times, as expected (Figure 6a and b). Some differences were observed only at the deflection voltages (VX3 ≃ ±180 V and VY3 ≃ 90 and 360 V) corresponding to the

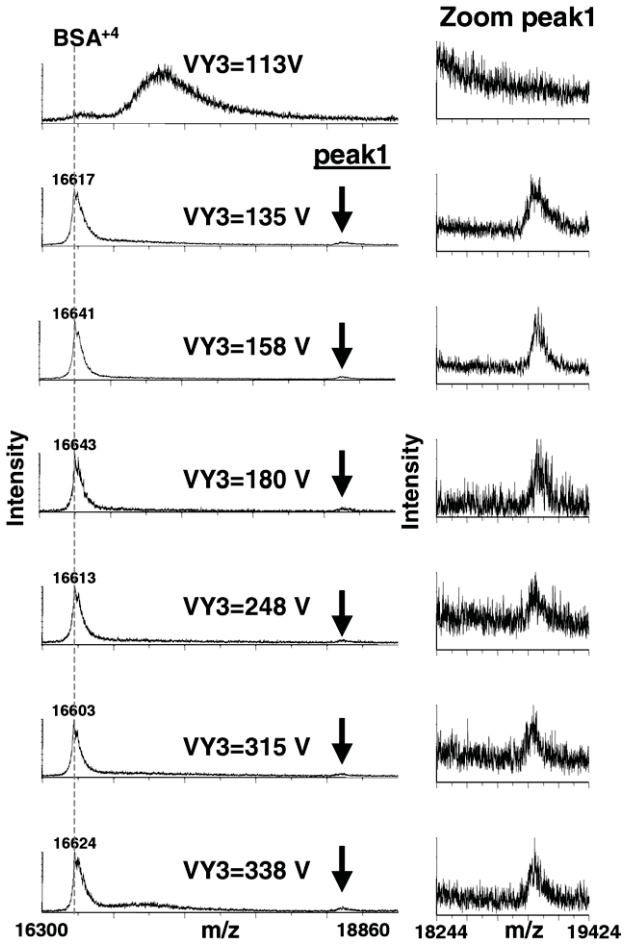

Figure 4. Partial positive ion MALDI mass spectra around the BSA^{+4} ion peak for different values of the vertical deflection voltage VY3. The dashed line shows the *m/z* expected for the free ion. Arrows show the position of the peak1 at the end of the high-mass tailing. The inserts show a zoom on peak1. Note: the peak1 is observed only when the BSA^{4+} free ion is detected.

limit of appearance-disappearance of the free ion and its decoupling with Distribution I. Typical time-of-flight mass spectra of singly charged apomyoglobin recorded at VX3 = −180 V are shown in Figure 6a. The relative abundance of Distribution I compared to that of the free ion strongly decreases when increasing the delay time. This effect was also found for other proteins (BSA, IgG1) and was more pronounced for the highest charge states (data not shown), which seems to indicate that a larger delay time promotes the decay-desolvation of protein-matrix cluster ions.

We did not notice this strong effect for the studied values of the vertical deflection voltages VY3. Figure 6b shows the time-of-flight mass spectra for BSA^{+1} acquired for VY3 = 360 V with different delay times. For the shorter delay time (dt = 180 ns), the free ion peak is discernable at the lower time-of-flight and the extent of the tail (Distribution I) is more important. At larger delay times, the free ion peak is weakly discernable and the tailing is less extended. This could indicate that short delay times would promote the formation of free ions as a result of collisions in a dense plume. However, the larger extent of Distribution I would indicate a lesser efficiency of analyte-matrix cluster decay.

The apparent contradiction of these results likely originates from the integrated signal over the detector area and the ion beam sampling versus the deflection voltage. Ions formed by different decay in the source and having different kinetic energy deficits can be simultaneously detected. As a result of this integration, the time-of-flight mass spectra show the average of ions produced by different decays. Of course, some weak heterogeneities of the ion beam before deflection can also be suspected. The VX3 range for free ions is in very good agreement with that expected from the ideal situation (pin-point beam), when the VY3 range upper bound is higher than that calculated.

The unknown size of the ion beam in the deflection region makes difficult any quantitative analysis of kinetic energy.

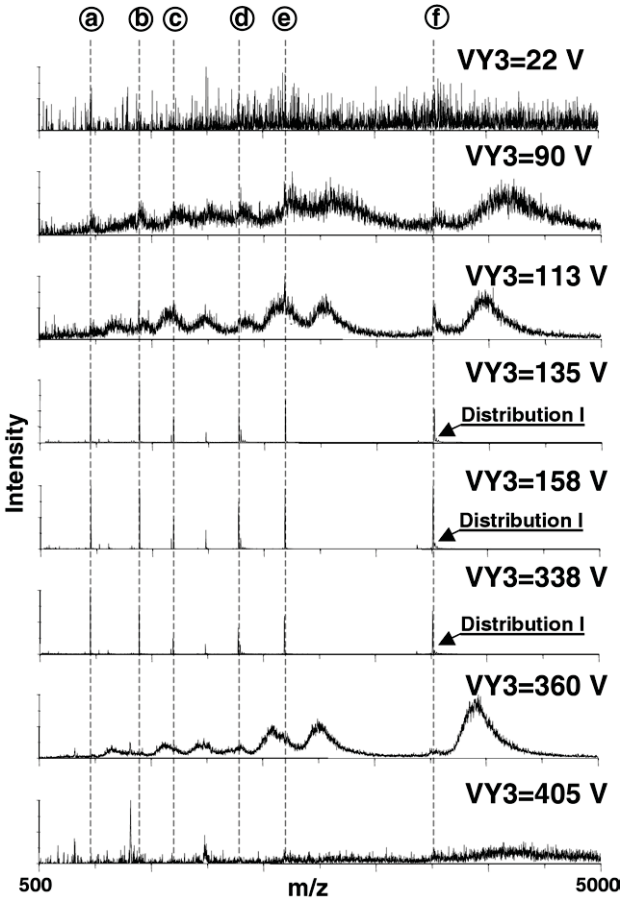

Figure 5. Positive-ion MALDI mass spectra of a mixture of six different peptides recorded for different values of the vertical deflection voltage VY3. The dashed lines show the *m/z* expected for these peptides, labeled from "a" to "f" [a: des-Arg1-Bradykinin; b: angiotensin I; c: Glu1-Fibrinipeptide B; d: ACTH (1–17); e: ACTH (18–39); and f: ACTH (7–38)]. HCCA was used as the matrix. The delay time was set to 180 ns.

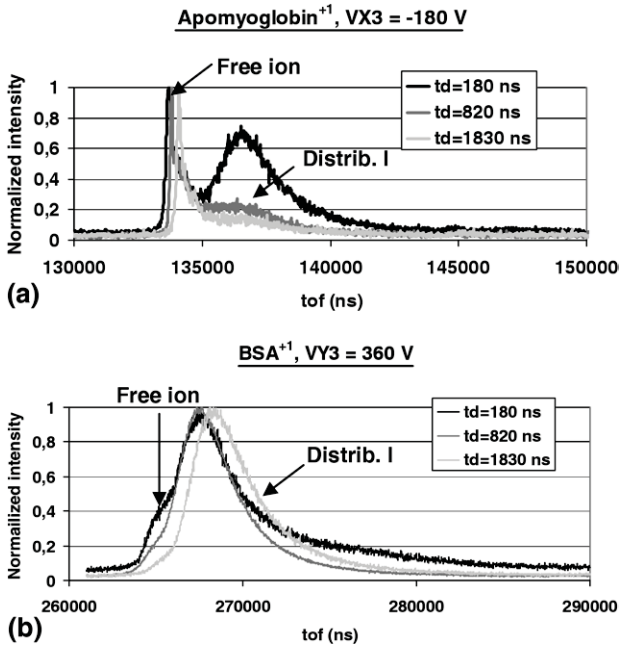

Figure 6. Positive-ion time-of-flight MALDI spectra recorded for (**a**) Apomyoglobin^{+1} and (**b**) BSA^{+1} using different delay times (td = 180, 820, or 1830 ns) for the deflection voltages VY3 = 360 V (BSA) and VX3 = −180 V (Apomyoglobin).

Tandem Mass Spectrometry (MS/MS) Experiments

These experiments were designed to study the noise appearing at higher *m/z* than that of the peptide free ions.

From the results described earlier, the ions resulting from a partial decay-desolvation of analyte-matrix clusters can be suspected to account for the tailing and noise beyond the analyte free ion peak. Even for peptides (ACTH 18–39 and ACTH 7–38), the free ion peak shows a tail of weak abundance (Figure 5). We verified that no satellite peaks (Na, K, matrix photochemical adducts) were detected for these peptides in the reflector mode.

Tandem mass spectrometry experiments were then performed to study the nature of ions contributing to the Distribution I for peptides. The time ion selector (TIS) was tuned to select the ion *m/z* within a window (−1 u, +10 u). MALDI-TOF-TOF mass spectra were recorded for different selected *m/z*, starting from the monoisotopic peak of the peptide up to a shift of *m/z* 400 toward higher masses, corresponding to the region of the high-mass tailing of the peptide (Distribution I).

Figure 7 shows typical tandem mass spectra recorded without gas in the collision cell for different selected *m/z* [referred to as "a" to "g" (Figure 7a) or "a" to "f" (Figure 7b)], the "parent ion" selection starting from the monoisotopic peak of ACTH 18–39 at *m/z* = 2465.3 (Figure 7a) or from the monoisotopic peak of ACTH 7–38 at *m/z* = 3657.9 (Figure 7b). A major feature of these MS/MS spectra is that the free peptide ion is always detected as a fragment for any *m/z* value of the "parent ion" selection. This peak appeared for a selection at every *m/z* shifted up to about 200 and 300 u for ACTH 18–39 and ACTH 7–38, respectively. The weak intensity of the peptide ion peak (Figure 7b) is due to the very weak signal (noise) selected for MS/MS experiments. In the MS/MS spectra, we did not find any ion exhibiting a series of characteristic losses consistent with a loss of either matrix molecules or fragments as previously reported by Krutchinsky and Chait [13].

The same experiments were performed with collision gas (N_2, 2×10^{-7} Torr). They showed that the peptide ion was always detected but with a smaller intensity, as expected (data not shown). However, the specific fragments of the peptide were detected only when the peptide *m/z* was selected. This was expected, taking into account the very low intensity (noise) in the selected windows.

These results clearly show that the chemical noise appearing at higher *m/z* beyond the peak of the free ion is composed of ions containing the peptide and results from the decay of peptide-matrix cluster ions in the source. Further desolvation of these clusters can occur in the drift tube. We verified for the different selected windows that the peptide ion signal decreased when using the deflection of metastable ion (metastable suppressor). This result proves that desolvation of peptide-matrix clusters takes place after the source 2 (Figure 1a).

We commonly observed in MALDI-TOF-TOF experiments on specific peptides with $m/z < 1500$ that besides the peptide fragment ions, specific fragments of matrix clusters are also detected. This is mainly due to the coexistence of peptide ions and matrix clusters ions in the same selected window. Although matrix ion signals in the selected *m/z* window cannot be distinguished, their very efficient fragmentation allowed some fragments to be detected.

Influence of Matrix and Laser Fluence

Some experiments in the linear mode were also carried out with SA as the matrix using the high mass analytes. Although studies were not so extensive with this matrix, trends concerning Distributions I and II were similar to those mentioned with HCCA.

The effect of the laser energy using HCCA was not systematically studied as a function of the deflection voltage. However, in the voltage range for pure ion detection, no major change was observed. We did not investigate the effect of the laser energy at the threshold (signal was too weak) nor at the highest values (possible detection saturation effect). Distribution I was present in a large laser energy range without appreciable variation of its abundance compared to that of the free ion.

Discussion

On the Origin of Distributions I and II

In this study on proteins, using the linear mode and radial deflection, we observed the presence of specific

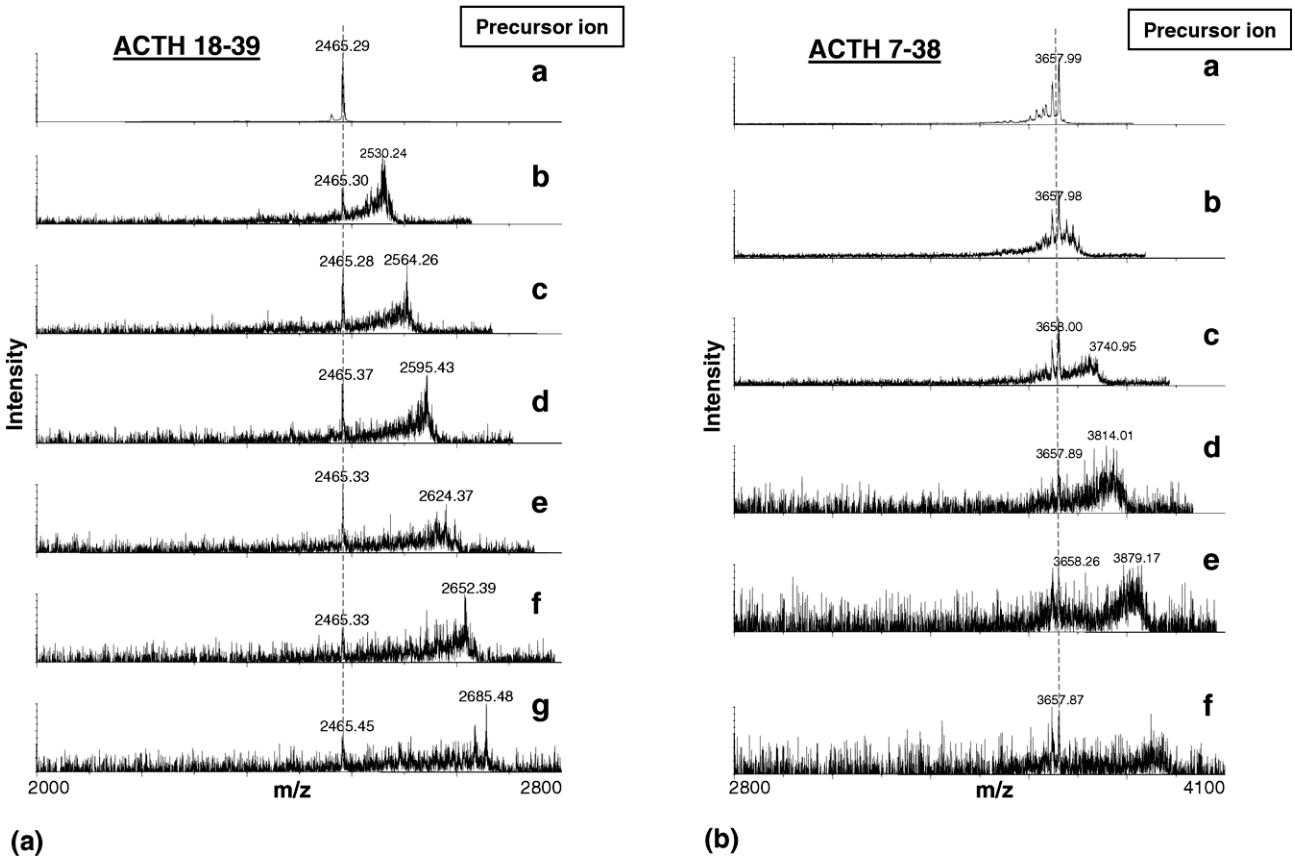

Figure 7. MALDI-TOF-TOF tandem mass spectra of the high-mass tail of peptides ACTH 18–39 (*m/z* 2465.2) and ACTH 7–39 (*m/z* 3657.9) without gas, recorded for different precursor ions within a window (−1 u, 10 u) (see text). (**a**) ACTH 18–39, for the following precursor ions: (a) *m/z* = 2465.2 (free ion is selected); (b) *m/z* = 2525.2; (c) *m/z* = 2555.2; (d) *m/z* = 2585.2; (e) *m/z* = 2615.2; (f) *m/z* = 2645.2; and (g) *m/z* = 2675.2. (**b**) ACTH 7–38 for the following precursor ions: (a) *m/z* = 3657.9 (free ion is selected); (b) *m/z* = 3687.9; (c) *m/z* = 3747.9; (d) *m/z* = 3807.9; (e) *m/z* = 3867.9; and (f) *m/z* = 3927.9. Dashed lines show the expected peak for singly charged ACTH 7–38 and 18–39 free ions.

features in the mass spectra, mentioned as Distributions I and II. It should be noted that some similar components associated with protein peaks or protein clusters peaks were already reported in linear TOF [7, 18, 19]. Distribution I was detected in the deflection voltage range of the free ion and beyond. It is a tailing of the free ion peak or a slightly decoupled broad peak. Ions forming such broad signals are characterized by higher time-of-flights and a low kinetic energy deficit. Distribution II appears for deflection voltage values only where no free ion was detected. It is a broad peak corresponding to ions with even more shifted time-of-flights and a larger kinetic energy deficit. The assumption that ions forming Distributions I and II resulted from the in-source decay of analyte-matrix clusters was confirmed by MALDI-TOF-TOF experiments. It was found that the chemical noise at higher *m/z* contained the free peptide ion. For proteins, the very high chemical noise around the free ion peak, forming Distributions I and II, likely originates from in-source decay-desolvation of analyte-matrix cluster ions. Simulations reported by Knochenmuss and Zhigilei [12] clearly indicate that stable clusters on a nanosecond scale are formed in the plume and that ions from these clusters are slowly released. Of course, the experimental conditions with the strong extracting field through the gradual velocity increase can be quite different.

Analyte Charge Effect

Two main processes can be invoked to account for the decreasing abundance of Distributions I and II with the increasing ion charge in linear mode (Figure 3b). The simpler would be that multiply charged ions of analyte-matrix clusters undergo a stronger desolvation within a short time after ejection (during proton transfer onto the analyte and/or collisions in the dense plume). The second would assume that the stronger acceleration of the multiply charged ions in the source stimulates the dissociation of weakly bonded matrix molecules. A desolvation process in-

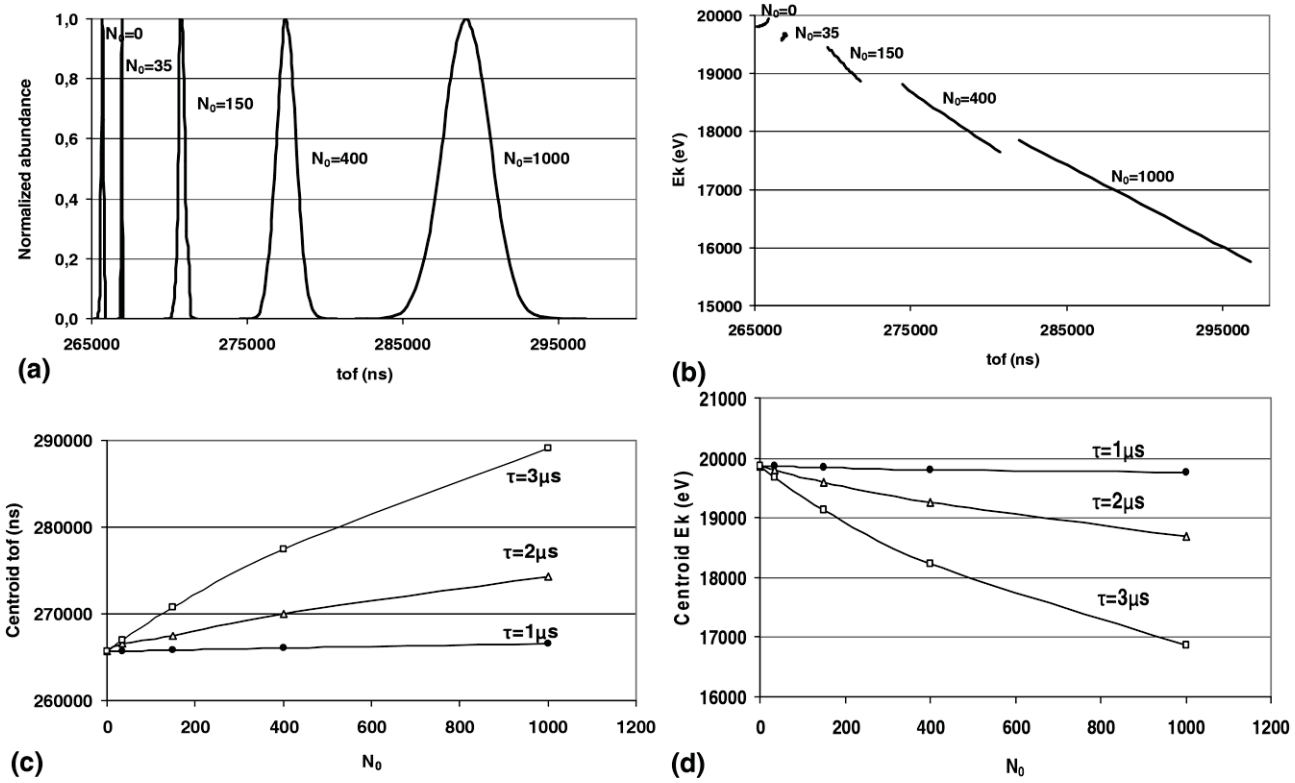

Figure 8. Model of a continuous in-source decay-desolvation of BSA-matrix cluster ions (z = 1). (**a**) Calculated time-of-flight (tof) spectra normalized to the highest abundance, using an initial number N_0 of matrix molecules and τ = 3 μs. (**b**) Kinetic energy (Ek) versus tof (τ = 3 μs). (**c**) Time-of-flight centroids as a function of the initial number of matrix molecules (N_0) and for different lifetimes (τ = 1, 2, 3 μs). (**d**) Kinetic energy (Ek) centroids as a function of the initial number of matrix molecules (N_0) and for different lifetimes (τ = 1,2,3 μs). The delay time was set to 1800 ns.

duced by transient high electric field variation was already mentioned [6, 9].

Analyte Mass Effect

The increasing abundance of the two distributions (I and II) with the mass increase of the analyte seems to be correlated to the analyte size. A larger external surface area of the analyte allows a larger number of matrix molecules to be attached.

Artifacts such as collisions of ions with metal surface or grid dispersion of ions cannot account for the ions of Distributions I and II. Indeed, all electrodes and grids are grounded along the tof tube in the linear mode and such fragment ions cannot reach the detector. Only radial deflection plates are set to lower voltages (<400 V) compared to the axial voltage (20,000 V) in the ion source.

Delayed Extraction

Two opposite decay-desolvation processes of the analyte-matrix ions were evidenced. One occurs for the short delay times and it is likely induced by collision in the dense plume. This implies that these clusters may originate from the deeper layers in the target. The other one occurs for the longer delay time and could account for clusters ejected from the uppermost layer of the sample without strong interaction with the plume. Both processes are present in the same ejection event.

Extension of Distributions I and II in the Mass Spectra of Proteins

Clearly any decay or desolvation of analyte-matrix cluster ions in the source produces ions with a larger time-of-flight and smaller kinetic energy compared to those of the free ion. However, it is not evident to predict to what extent they contribute to the TOF spectra. Simple models were developed to gain a better insight of such a decay-desolvation.

The possibility that analyte-matrix cluster ions can be formed in the plume cannot be discarded [20]. If they are formed before the delayed extraction, they are similar in principle to ejected clusters.

Continuous model. The initial analyte-matrix clusters, containing one analyte molecule (M_a) and N_0 matrix molecules (M_m), were assumed to decay according to a simple law driven by a lifetime τ. The τ parameter can account for a natural desolvation and/or collision-

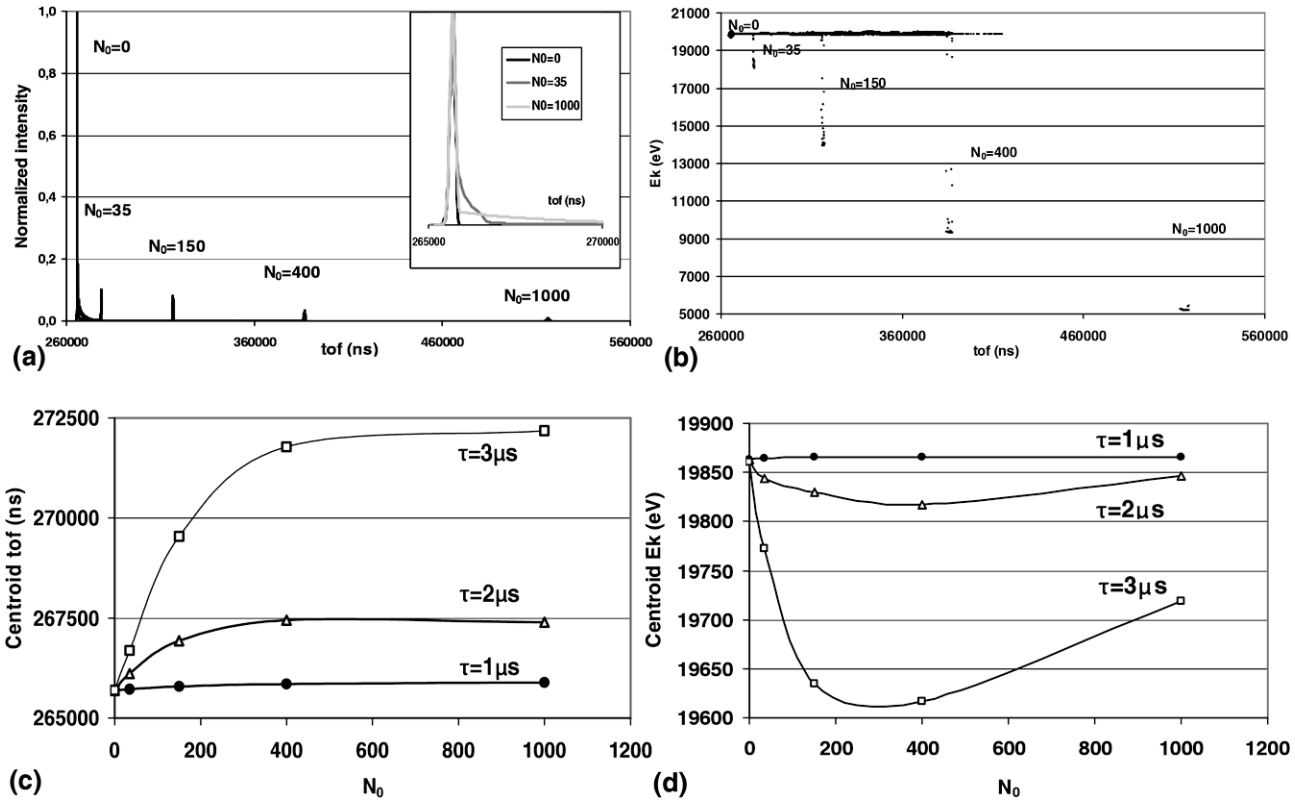

Figure 9. Model of a discontinuous decay-desolvation of BSA-matrix cluster ions (z = 1). (**a**) Calculated time-of-flight spectra normalized to the highest abundance, using an initial number N_0 of matrix molecules. The insert shows the magnification of the tof spectra in the range of the pure BSA^{+1} free ion for N_0 = 35 and 1000. (**b**) Kinetic energy versus time-of-flight (t = 3 μs). (**c**) Time-of-flight centroids as a function of the initial number matrix molecules N_0 and for different lifetimes (τ = 1, 2, 3 μs). (**d**) Kinetic energy centroids as a function of the initial number matrix molecules N_0, for different lifetimes τ (τ = 1, 2, 3 μs). The delay time was set to 1800 ns.

induced decay-desolvation. Time-of-flight and kinetic energy were calculated (custom-made program) taking into account the mass of the cluster [$M_{clust} = M_a + M_m N_0 \exp(-t/\tau)$], the isotopic pattern (isotopes with abundance >1% of the most abundant isotope were used), the two-stage ion source geometry, and the delay time. The initial axial velocity distribution was assumed to be Gaussian (for HCCA V_0 = 350 m/s and full width at half-maximum = 150 m/s) and 21 values were considered from 20 to 680 m/s. Figure 8a shows typical time-of-flight spectra calculated for BSA^{+1} using τ = 3 μs and a delay time (td) = 1800 ns for initial clusters containing 0 (free ion), 35, 150, 400, or 1000 matrix molecules. For the free ion, the acceleration time in the first stage of the source is 3.82 μs. Figure 8b shows the range of ion kinetic energy for different numbers of matrix molecules (N_0) attached to the analyte. Increasing the initial size of the clusters results in a strong shift and broadening of the peak and a large kinetic energy deficit. The centroids of the time-of-flight peaks and of the kinetic energy distributions are shown in Figure 8c and d, respectively, for τ = 1, 2, and 3 μs. These calculations can partly account for the observed Distribution II in the deflection experiments (Figure 2a). The time-of-flight shift for VY3 = 45 V (Figure 2a) can be fitted by the decay-desolvation of a cluster initially with N_0 = 500 matrix molecules and with a lifetime τ = 3 μs. However, they cannot easily explain Distribution I. The decay-desolvation of different clusters (N_0, τ) has to be considered. The time-of-flight shift observed at VY3 = 248 V (not shown in Figure 2a) can be fitted with N_0 = 35 (τ = 3 μs) and N_0 = 90 (τ = 2 μs) with a kinetic energy deficit (170–200 eV). At VY3 = 338 V (Figure 2a), it fits with N_0 = 75 (τ = 3 μs) and N_0 = 225 (τ = 2 μs) with a kinetic energy deficit of about 400 eV.

Discontinuous model. The starting point of this model was to consider the role of the extracting field on the possible stimulated desolvation of analyte-matrix cluster ions [7, 9]. It could also account for collision in the dense plume of the analyte-matrix clusters with other matrix clusters. The initial cluster, $M_{clust} = M_p + N_0 M_m$, was assumed to be completely desolvated at a time t with a probability $p \simeq p_0 \exp(-t/\tau)$. The time-of-flight and kinetic energy were calculated as mentioned earlier. Figure 9a shows for BSA^{+1} that the mass spectrum is composed of the free ion peak with a tailing and a peak shifted toward higher time-of-flight. The free ions

result from the fast desolvation before extraction, the tail results from in source desolvation, and the shifted peak results from the absence of in-source desolvation. The extension and abundance of the tail (see insert in Figure 9a) increase with the number of matrix molecules in the initial cluster. The kinetic energy range is large (Figure 9b). However, the centroids over the entire time-of-flight and kinetic energy ranges are rather close to those of the free ion peak (Figure 9c and d). This model can account for only Distribution I and peak1. The peak1 would originate from the analyte-matrix clusters surviving in the source. Some "pockets" or folded regions of the protein could trap matrix molecules during crystallization of the target.

We are aware that these simple models cannot in principle depict in detail the complex phenomena occurring in the expanding plume [9, 12]. In addition, they cannot account for a complete description of the ion trajectories, especially in a real time-of-flight mass spectrometer, which is out of reach. They modestly intend to give some orders of magnitude of the analyte-matrix clusters in source decay and to account qualitatively for the experimental trends.

Conclusion

Results presented in this article clearly show that desolvation or decay of analyte-matrix cluster ions occurs in the MALDI source. High-mass tailing and shifted peaks were found to account for such ions in the linear mode. Deflection experiments also indicate that these ions have a kinetic energy deficit. These decay processes are responsible for the chemical noise beyond the protein peak. This was confirmed by the MALDI-TOF-TOF experiments on the high-mass tail of peptides.

The importance of these decay-desolvation processes increases with the mass but decreases with the charge of the protein.

All these results lead to new questions on the role of the target preparation in the production of such analyte-matrix clusters. We are currently working on the in-solution characterization of protein-matrix clusters before deposition to evaluate whether proteins are co-crystallized as pure or as a preformed protein-matrix cluster.

These experiments gave similar results for two popular matrices (HCCA and SA). Other experiments have to be performed with 2,5-DHAP, considered as a very "soft" matrix [21].

Reducing the noise is an important challenge to gain a better analysis of the MW of entire proteins. One possible way would be to add energy filters along the time-of-flight axis.

Acknowledgments

The authors thank Le Conseil Régional de Ile de France and Drs. Gérard Chassaing and Germain Trugnant (Réseau Physique-Chimie-Biologie-Médecine) of the Pierre and Marie Curie University for supporting grants of the mass spectrometry equipment of the Plateform. They also thank Bernard Oudart from Apellera France for his useful help and contributing his knowledge of the MALDI-TOF-TOF apparatus.

References

1. Karas, M.; Bachmann, D.; Bahr, U.; Hillenkamp, F. Matrix-Assisted Ultraviolet Laser Desorption of Non-Volatile Compounds. *Int. J. Mass Spectrom.* **1987,** *78,* 53–68.
2. Georgiou, S.; Hillenkamp, F. Laser Ablation of Molecular Substrates. Special Issue. *Chem. Rev.* **2003,** *103,* 349–393.
3. Horneffer, V.; Glückmann, M.; Krüger, R.; Karas, M.; Strupat, K.; Hillenkamp, F. Matrix-Analyte Interaction in MALDI-MS: Pellet and Nano-Spray Preparations. *Int. J. Mass Spectrom.* **2006**, *249–250,* 426–432.
4. Trimpin, S.; Räder, H.; Müllen, K. Investigations of Theoretical Principles for MALDI-MS Derived from Solvent-Free Sample Preparation. Part I. Preorganization. *Int. J. Mass Spectrom.* **2006,** *253,* 13–21.
5. Karas, M.; Gluckmann, M.; Schafer, J. Ionization in Matrix-Assisted Laser Desorption/Ionization: Singly Charged Molecular Ions Are the Lucky Survivors. *J. Mass Spectrom.* **2000,** *35,* 1–12.
6. Fournier, I.; Brunot, A.; Tabet, J. C.; Bolbach, G. Delayed Extraction Experiments Using a Repulsive Potential before Ion Extraction: Evidence of Clusters as Ion Precursors in UV-MALDI. Part I: Dynamical Effects with the Matrix 2,5-Dihydroxybenzoic Acid. *Int. J. Mass Spectrom.* **2002,** *213,* 203–215.
7. Fournier, I.; Brunot, A.; Tabet, J. C.; Bolbach, G. Delayed Extraction Experiments Using a Repulsing Potential before Ion Extraction: Evidence of Non-Covalent Clusters as Ion Precursor in UV Matrix-Assisted Laser Desorption/Ionization. Part II—Dynamic Effects with alpha-Cyano-4-Hydroxycinnamic Acid Matrix. *J. Mass Spectrom.* **2005,** *40,* 50–59.
8. Karas, M.; Kruger, R. Ion Formation in MALDI: The Cluster Ionization Mechanism. *Chem. Rev.* **2003,** *103,* 427–440.
9. Itina, T. E.; Zhigilei, L.; Garrison, B. Microscopic Mechanisms of Matrix Assisted Laser Desorption: Insights from Molecular Dynamics Simulation. *J. Phys. Chem. B* **2002,** *106,* 303–310.
10. Zhigilei, L. V.; Leveugle, E.; Garrison, B. J.; Yingling, Y. G.; Zeifman, M. I. Computer Simulations of Laser Ablation of Molecular Substrates. *Chem. Rev.* **2003,** *103,* 321–348.
11. Knochenmuss, R.; Zenobi, R. MALDI Ionization: The Role of In-Plume Processes. *Chem. Rev.* **2003,** *103,* 441–452.
12. Knochenmuss, R.; Zhigilei, L. V. Molecular Dynamics Model of Ultraviolet Matrix-Assisted Laser Desorption/Ionization Including Ionization Processes. *J. Phys. Chem. B* **2005,** *109,* 22947–22957.
13. Krutchinsky, A. N.; Chait, B. T. On the Nature of the Chemical Noise in MALDI Mass Spectra. *J. Am. Soc. Mass Spectrom.* **2002,** *13,* 129–134.
14. Dreisewerd, K. The Desorption Process in MALDI. *Chem. Rev.* **2003,** *103,* 395–426.
15. Beavis, R. C.; Chait, B. T. Cinnamic Acid Derivatives as Matrices for Ultraviolet Laser Desorption Mass Spectrometry of Proteins. *Rapid Commun. Mass Spectrom.* **1989,** *3,* 432–435.
16. Yergey, A. L.; Coorssen, J. R.; Backlund, P. S., Jr.; Blank, P. S.; Humphrey, G. A.; Zimmerberg, J.; Campbell, J. M.; Vestal, M. L. De Novo Sequencing of Peptides Using MALDI/TOF-TOF. *J. Am. Soc. Mass Spectrom.* **2002,** *13,* 784–791.
17. Vestal, M. L.; Campbell, J. M. Tandem Time-of-Flight Mass Spectrometry. *Methods Enzymol.* **2005,** *402,* 79–108.
18. Kinsel, G. R.; Edmondson, R. D.; Russell, D. H. Profile and Flight Time Analysis of Bovine Insulin Clusters as a Probe of Matrix-Assisted Laser Desorption/Ionization Ion Formation Dynamics. *J. Mass Spectrom.* **1997,** *32,* 714–722.
19. Livadaris, V.; Tabet, J. C.; Blais, J. C. Formation of Non-Specific Protein Cluster Ion in Matrix-Assisted Laser Desorption/Ionization: Abundances and Dynamical Aspects. *Eur. J. Mass Spectrom.* **2000,** *6,* 409–413.
20. Kristyan, S.; Bencsura, A.; Vertes, A. Modeling the Cluster Formation during Infrared and Ultraviolet Matrix-Assisted Laser Desorption Ionization of Oligonucleotides in Succinic Acid Matrix with Molecular Mechanics. *Theor. Chem. Acc.* **2002,** *107,* 319–325.
21. Wenzel, T.; Sparbier, K.; Mieruch, T.; Kostrzewa, M. 2,5-Dihydroxyacetophenone: A Matrix for Highly Sensitive Matrix-Assisted Laser Desorption/Ionization Time-of-Flight Mass Spectrometric Analysis of Proteins Using Manual and Automated Preparation Techniques. *Rapid Commun. Mass Spectrom.* **2006,** *20,* 785–789.